Journal of Engineering and Applied Sciences 12 (3): 593-601, 2017
ISSN: 1816-949X

Automated Annotation System for Hemorrhage Slices

[1]Hau Lee Tong, [2]Mohammad Faizal Ahmad Fauzi, [1]Su Cheng Haw,
[1]Tzen Vun Timothy Yap and [1]Hu Ng
[1]Faculty of Computing and Informatics,
[2]Faculty of Engineering, Multimedia University, 63100 Cyberjaya, Selangor, Malaysia

Abstract: The main objective is to annotate and classify different types of hemorrhagic slices such as intra-axial, subdural and extradural slices. A two-segregated annotation is proposed to classify hemorrhagic slices due to their different shapes and locations in the brain. The first annotation is to identify the intra-axial hemorrhage slice whereas the second annotation is to classify the subdural and extradural slices. All the extracted features from both annotations will be used as inputs to the Support Vector Machine (SVM) classifier. Experiments conducted on a set of 519 CT slices under the proposed method show significant results. From the findings, the proposed method yields 79.3, 85 and 89.2% correct classification rate for intra-axial, subdural and extradural. On overall, the CCR obtained for subdural and extradural slices is higher than intra-axial slices. This is contributed by more specific local shape features are employed for subdural and extradural which results in better recognition. Global features are adopted to classify the intra-axial slices due to their arbitrary shapes. The proposed approach can be used to create an automated retrieval system so that radiologists and medical students can use it to retrieve the hemorrhage images for further study and analysis.

Key words: Hemorrhage annotation, subdural, extradural, intra-axial, retrieve the hemorrhage

INTRODUCTION

Computed Tomography (CT) scanner appears to be a vital tool in the assessment of patients with head trauma. It remains the investigation of choice even following the advent of MRI, due to the ease of monitoring of injured patients and the better demonstration of fresh bleeding. The detection of the hemorrhage is significant so that immediate and proper treatment can be carried out.

An annotation system of the hemorrhages can assist the radiologist in identifying the hemorrhage and reaching at a decision faster. Different approaches have been presented by researchers to achieve better detection accuracy. Human head is roughly bilateral symmetric. Thus, the human head can be divided into left and right hemispheres. Both cerebrum and cerebellum are symmetric with lobes and ventricles in both hemispheres. Brain hemorrhage can cause brain shift. As such investigation of the symmetric information can assist hemorrhage detection. Matesin *et al*. (2001) proposed a rule-based approach to detect brain lesions. Firstly, the symmetry axis of the head is located by using several moments. Then a rule-based expert system is developed to annotate the lesions and so on. Likewise, a knowledge-based approach and midline location was also adopted by Chan (2007). Besides Liu *et al*. (2004) proposed a symmetric detection approach to detect the brain lesions by identifying the symmetry of each CT slice. If the midline is shifted then hemorrhage is considered to exist. Similar midline detection approach was also adopted by Chawla *et al*. (2009).

Besides symmetric comparison, global features are extracted from the entire slices and SVM technique is applied by Liu *et al*. (2008) for the hemorrhage slices detection. Gong *et al*. (2007) proposed region-based feature extraction in which region features such as area, eccentricity, extent and so on are extracted and subsequently, trained decision tree is adopted to differentiate normal regions with different types of hemorrhagic regions. However, trained decision tree produces relatively low accuracy for hemorrhages as compared to normal regions. Likewise, Ramana and Korrapati also proposed local region feature extraction but with neural network supervised classification to classify different types of hemorrhages.

Corresponding Author: Hau Lee Tong, Faculty of Computing and Informatics, Multimedia University, 63100 Cyberjaya, Selangor, Malaysia

The main objective of this research is to design and propose an automated retrieval system so that radiologists and medical students can use it to retrieve the hemorrhage images for further study and analysis. In this study, annotations were performed to classify intra-axial, subdural and extradural slices. The main contributions of this study are two annotation processes are introduced to classify and detect different types of hemorrhagic slices.

Besides, for intra-axial slices annotation, a novel midline approach is proposed. In addition, new shape features for annotation of subdural and extradural are also proposed.

MATERIALS AND METHODS

This study elaborates on two-level image enhancement, parenchyma extraction, clustering and annotation processes for the proposed methodology.

Original image enhancement: The original image lacks of dynamic range whereby only certain objects are visible as shown in Fig. 1a. Therefore, the first process is to expand the dynamic range to the desired range to improve the visibility of the ROIs. The automated contrast stretching system is proposed to achieve this. This is significant to fit the contrast of all the original images into the desired range.

The proposed automated contrast stretching operates as below: firstly the histogram for the original image is constructed as shown in Fig. 1b. The constructed histogram consisted of several peaks whereby the leftmost and rightmost major peaks are contributed by the background and ROIs, respectively. Then, the smoothing process is performed where convolution operation with a vector (value of 10-3) is applied. The smoothing process is to facilitate the acquisition process of appropriate upper and lower limits. The smoothened curve is transformed into absolute first difference (ABS) as shown in Fig. 1c. The closest peak on the left and right is auto-determined as the lower limit, IL and upper limit, IU, respectively. The acquired IL and IU are utilized for the linear contrast stretching as shown in Eq. 1:

$$F(i, j) = I_{max} \frac{(I(i, j) - I_L)}{(I_U - I_L)} \quad (1)$$

where, I_{max}, I(i, j) and F(i, j) denote the maximum intensity of the image, pixel value of the original image and pixel value of the contrast improved image, respectively. After contrast stretching, the enhanced image is shown in Fig. 1d.

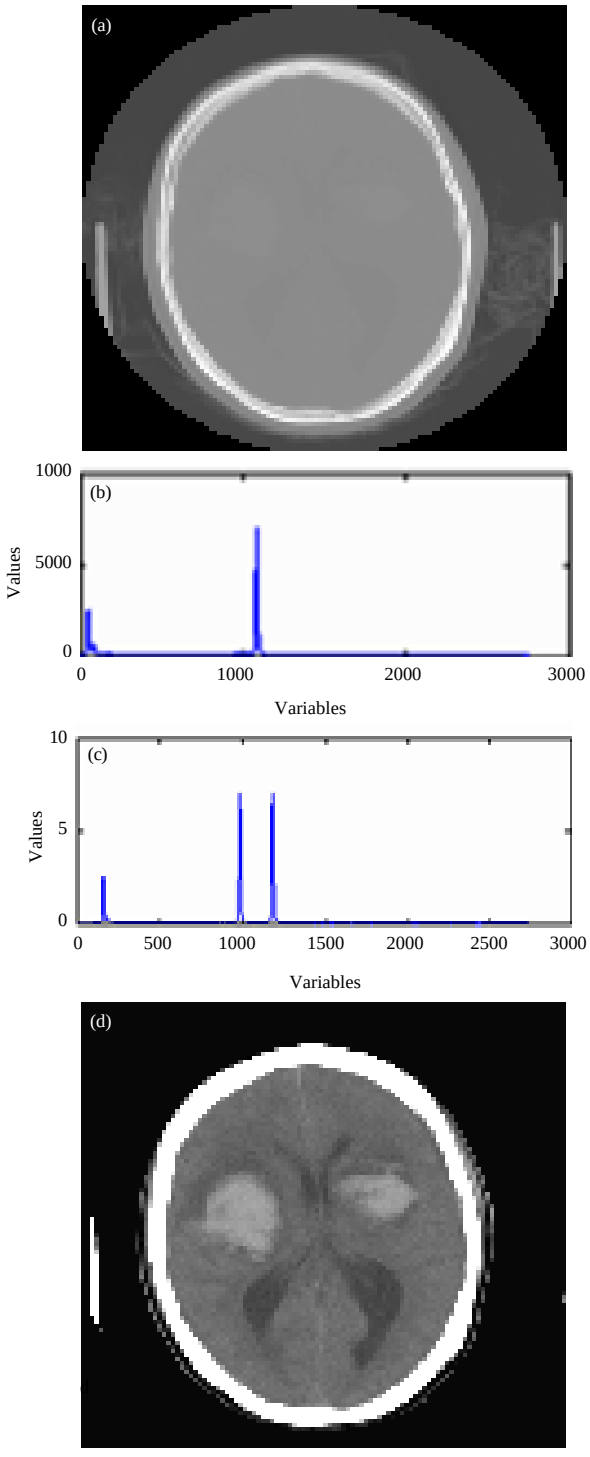

Fig. 1: a) Original image; b) Absolute first difference; c) Constructed histogram and d) Enhanced image

Parenchyma extraction: The second process is to extract the parenchyma from the enhanced image. In order to obtain the parenchyma, thresholding technique is utilized to alienate the background, skull and scalp from it. Generally, the skull always appears to be the largest connected component compared with the objects in the background. Therefore, the largest connected component is pinned down in order to obtain the skull. After that, parenchyma mask is generated by filling up the hole inside the skull. Lastly, intensity of the skull is set to zero and the parenchyma is acquired.

Hemorrhagic regions contrasts stretching: This process is important to make the hemorrhagic regions more visible to clearly reveal the dissimilarity between the hemorrhagic hemisphere and non hemorrhagic hemisphere. Most of the previous works focus on the images without hemorrhagic regions contrast stretching. However, from our discovery the contrast enhanced hemorrhagic slices reflected better dissimilarity in terms of the intensity for the left and right hemispheres. This directly alleviates the classification process. The range of the contrast is stretched based on a priori knowledge that intensity of the hemorrhage is beyond the peak intensity of the images. As such contrast stretching is emphasized on the higher intensity to enhance visibility of the hemorrhagic regions. Prior to the contraststretching, the appropriate lower and upper limits needed to be obtained. The acquisition of the lower and upper limits is automatically obtained by the following steps:

- Construct the histogram for the acquired parenchyma
- Identify the lower limit, IL which is peak position of the constructed histogram. From the obtained lower limit, the upper limit can be derived by Eq. 2:

$$i_u = I_L + I_e \quad (2)$$

where, I_e is predefined at 500 found from experimental observation:

- Subsequently, input the auto-determined values of IU and IL into Eq. 1 for the contrast stretching
- Lastly, apply the median filter to reduce the "salt and pepper" noise that appear in the acquired image. The image after the contrast stretching and "salt and pepper" noise reduction is shown in Fig. 2

Potential hemorrhagic region clustering: The aim for this reseach is to cluster potential hemorrhagic regions into a single cluster. In order to achieve this, firstly, the image is partitioned into two clusters. From these two clusters, the low intensity cluster without potential hemorrhagic regions is ignored. Only the high intensity cluster which consists of potential hemorrhagic regions is considered. In other words, the high intensity cluster can consists of high intensity normal regions and hemorrhagic regions. Prior to the classification of intra-axial, subdural and extradural, the regions will be further divided into boundary regions and intra regions.

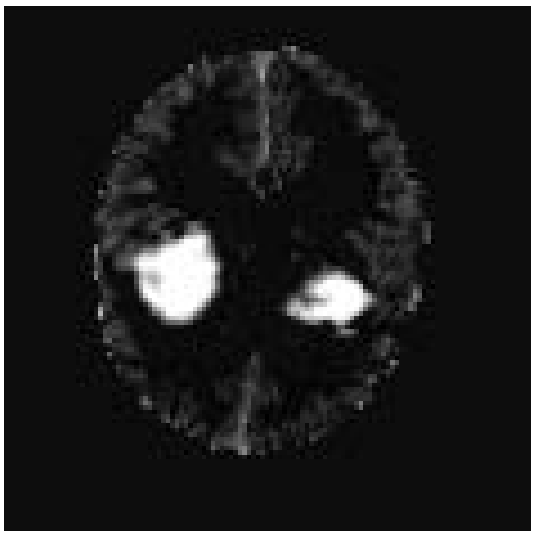

Fig. 2: Hemorrhagic enhanced image

Four clustering techniques which are Otsu thresholding, Fuzzy C-Means (FCM), k-means and Expectation-Maximization (EM) are attempted in order to select the most appropriate technique for subdural, extradural and intra-axial hemorrhages annotation. The comparison results are shown in Fig. 3. From the results obtained, Otsu thresholding, FCM and EM encountered over-segmentation as hemorrhagic region is merged together with surrounding pixels and more noises are present. This directly causes the hemorrhagic region to be distorted from their original shape. On the other hand, k-means conserves the original shape most of the time and produces less noise. This contributes for more accurate region properties acquisition at the later region-based feature extraction. Thus, k-means clustering is adopted in order to obtain better annotation results.

Annotation process of intra-axial hemorrhage slice: In this study, the boundary regions which have contact with the skull will be removed from the higher intensity cluster. As a result, the images with purely intra regions will be acquired for the annotation of intra-axial hemorrhage slice.

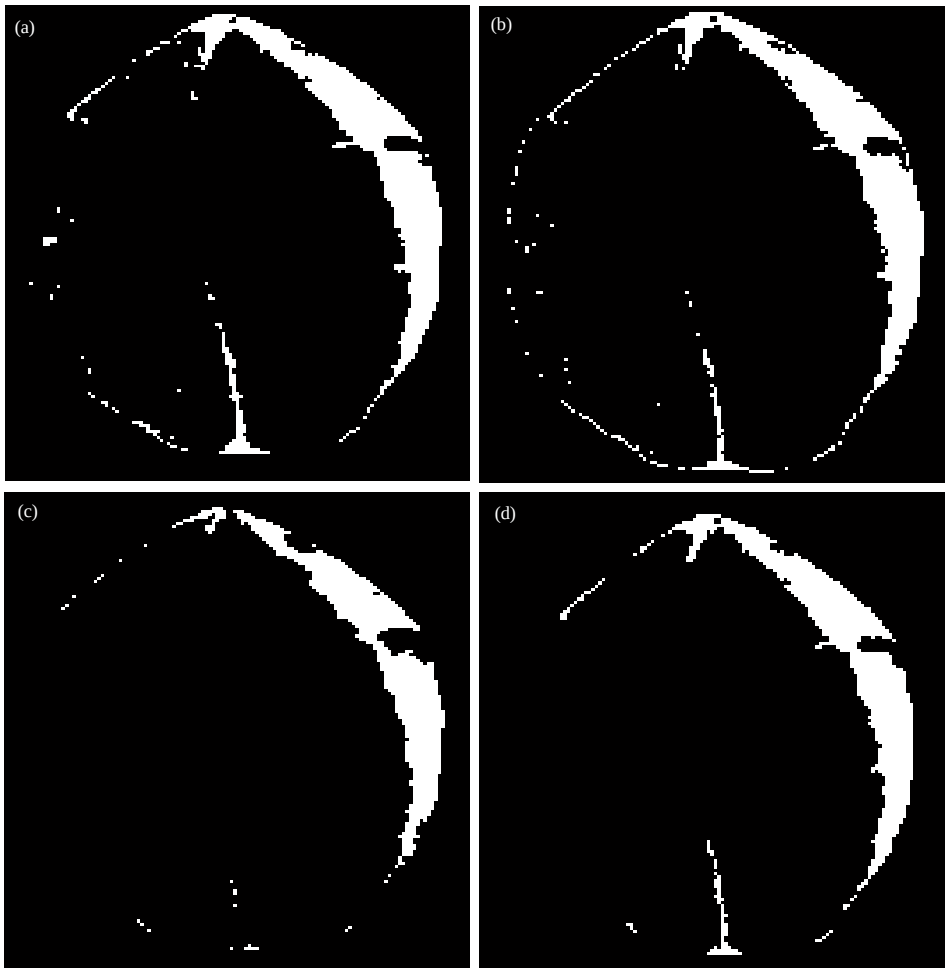

Fig. 3: a) Clustering results by Otsu thresholding; b) FCM clustering; c) K-means clustering and d) EM clustering

Parenchyma midline acquisition approach: So, far we have attempted two approaches in order to acquire the parenchyma midline based on the parenchyma's contour. First approach basically is to form the midline from the midpoints by using least squares linear regression. Firstly, midpoints are obtained from the constructed horizontal lines for the parenchyma contour. Then vertical midline is acquired by using least squares linear regression as given by Eq. 3:

$$y = b_0 + b_1 x \quad (3)$$

Where:

$b_1 = \Sigma[(x_i-x)(y_i-y)]/\Sigma[(x_i-x)^2]$

$b_0 = y-b_1*x$

The second approach of the parenchyma midline acquisition consists of two stages. Firstly, line scanning is proposed to locate the two points of interest which are frontal crest and internal occipital protuberance. From these two points, midline can be established in order to segregate parenchyma into left and right hemispheres. In the cases that points of interest are not found, a second stage process will be executed. For the second stage, Radon transform cum moving average is proposed to locate the two points of interest. The overall process for the second approach midline acquisition is listed as following:

- Firstly, acquire the contour of the parenchyma as shown in Fig. 4a
- Then, use two bounding boxes to obtain the bottom and top sub-contours from the acquired contour from (i) as shown in Fig. 4b-c

Execute the line scanning process: The scanning begins from the endpoints of the top and bottom sub-contours to locate the local minima and local maxima (x1, y1) for bottom sub-contour is as shown in Fig. 4b.

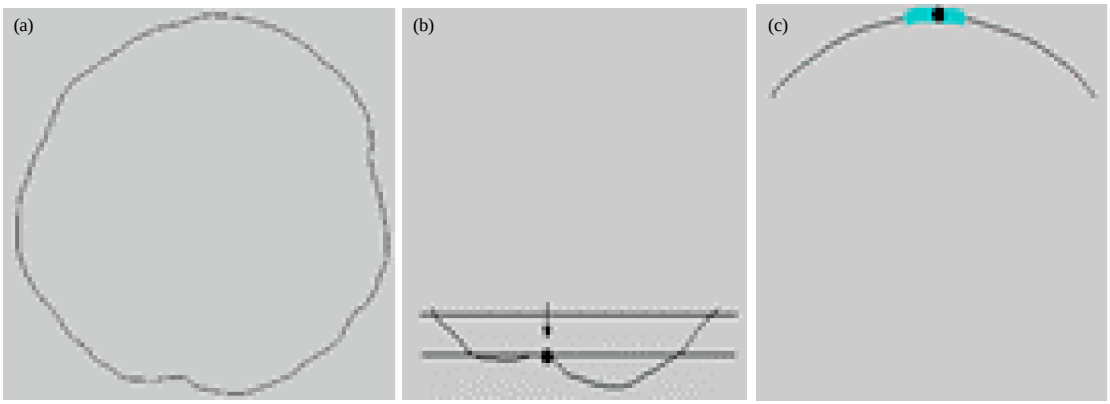

Fig. 4: a) Contour of intracranial area; b) Bottom sub-contour with the with the detected local maxima and c) Top sub-contour with the located highest average value of intensity point

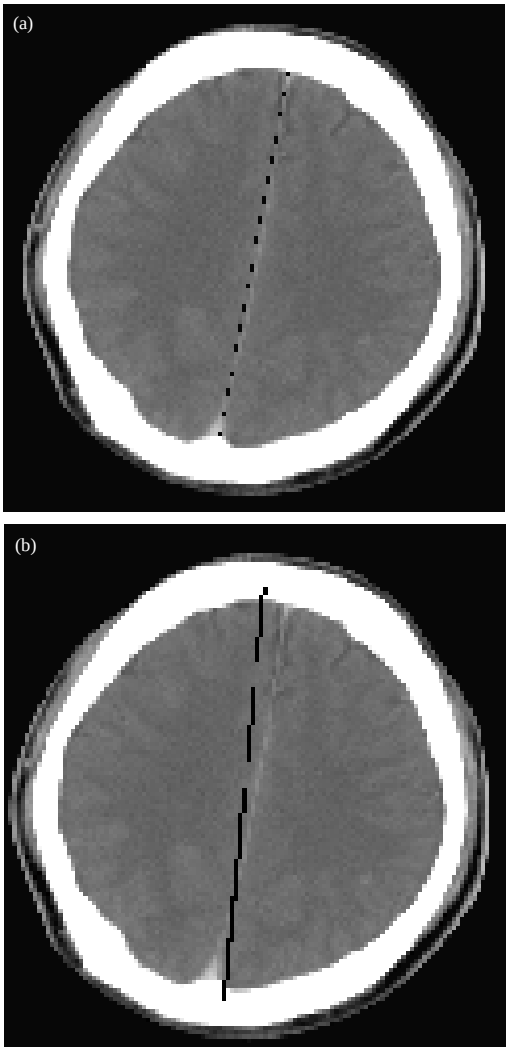

Fig. 5: a) Detected midline by first approach and b) Detected midline by second approach

In the case where the local minima or maxima point is not found, radon transform is utilized to shorten the searching line. Radon transform8 is defined as:

$$R(\rho,\theta) = \iint f(x,y)\delta(\rho - x\cos\theta - y\sin\theta)\,dxdy \quad (4)$$

where, ρ, θ and f (x, y) denote distance from origin to the line, angle from the X-axis to the normal direction of the line and pixel intensity at coordinate (x, y). Dirac delta function is represented by δ (·). From our experimental observation θ is fixed at 170°. As a result, the obtained shortened line is thickened as depicted in Fig. 4c. Apply the moving average to locate the points of interest (x_2, y_2) from the shortened contour line. Basically moving average is used for the computation of the average intensity for all the points along the contour line. The location of the points is based on the highest average value of intensity as shown in Fig. 4c. Eventually, midline is established by using the linear interpolation as defined in Eq. 5:

$$y = y_1 + \frac{(x - x_1)(y_2 - y_1)}{(x_2 - x_1)} \quad (5)$$

From the experimental results as observed in Fig. 5, the second approach has more accurately located midline and is more robust for the different parenchyma's shape. Therefore, the second approach is adopted to divide the parenchyma to the left and right hemispheres.

Feature extraction: The located midline from previous section is employed to segregate the parenchyma into left and right hemispheres. Then 22 features are extracted from both hemispheres for the first stage classification. The dissimilarity of each feature for the left and right

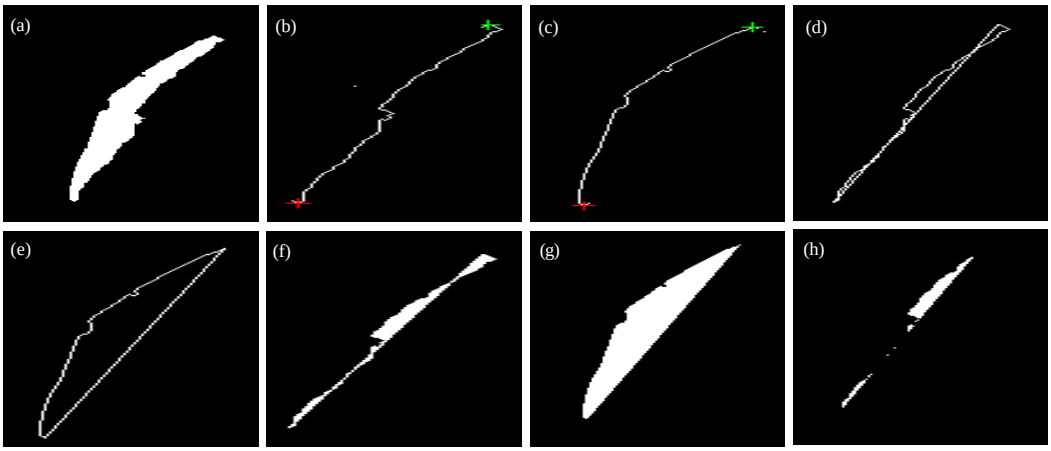

Fig. 6: a) SDH region; b) Inner contour with located endpoints; c) Outer contour with located endpoints; d) Inner closed contour; e) Outer closed contour; f) Filled up inner contour; g) Filled up outer contour and h) Overlapping area

hemispheres is computed by using euclidean distance. In general, the higher the dissimilarity, the higher the possibility a slice appears to be intra-axial hemorrhagic slice. Thus, the adopted features are based on their significant contribution in terms of dissimilarity for distinguishing the normal slices with the intra-axial hemorrhage slices. The first feature considered is entropy which is a statistical measure of randomness that uses to characterize the texture of the slices. Entropy is defined as:

$$\text{Entrop} = -\sum_{i} P_i \log_2 P_i \quad (6)$$

where, P_i is the probability that the difference between two adjacent pixels is equal to I. The second measure adopted is the edge histogram. Four-bin edge histogram which furnishes four features is employed to represent the strength of edges in 0, -45, 45 and 90° directions for the left and right hemispheres. The 4-bin edge histogram is constructed based on the following steps:

- Compute the image gradients which are vertical gradient, G_x and horizontal gradient, G_y by using the following Sobel operators:

  Sobel operator for G_y = [1 2 1; 0 0 0; -1 -2 -1];
  Sobel operator for G_x = [-1 0 1; -2 0 2; -1 0 1]

- For each edge pixel for both hemispheres, compute the edge direction based on Eq. 7:

$$\theta = \arctan\left(\frac{Gy}{Gx}\right) \quad (7)$$

- The edge direction is then quantized into four bins for respective direction
- Lastly, the edge histogram is normalized with respect to the image size in which each bin value reflects the percentage of a certain edge in the image

Another histogram we considered is intensity histogram which is based on the hemorrhage contrast enhanced image. Likewise, histograms of intensities are constructed for the left and right hemispheres. From priori knowledge, intensity of the hemorrhage is located after the peak intensity of the first level image enhancement image. Therefore bins of interest are high indexed bins. To obtain the high indexed bins, the histograms are thresholded based on the lower limit, IL obtained during hemorrhagic regions contrast stretching.

Prior to the extraction of the last batch textural features, the co-occurrence matrix is calculated on both hemispheres. Haralick (1997) proposed the use of the Gray Level Co-occurrence Matrices(GLCM) for the description of the texture features. For our case, co-occurrence matrices for 0, 45, 90 and 135° are computed to achieve a degree of rotational invariance. Four textural measures which are energy, entropy, autocorrelation and maximum probability are considered which contribute sixteen features for four directions.

Annotation process of subdural and extradural slices: In this research, only boundary regions are considered for the annotation of the subdural and extradural slices. Prior to the slice annotation, properties of each boundary region will be extracted for the classification of normal, subdural or extradural region. As long as subdural or extradural region is detected in the slice that particular slice will be annotated as subdural or extradural slice.

Radiologists usually determine the subdural and extradural regions based on their intensity, size, shape and position. In this stage, the features are considered based on two criteria which are to distingush normal regions from subdural and extradural regions and subdural from extradural. The 11 shape features adopted are region area, border contact area, orientation, linearity, concavity, ellipticity, circularity, triangularity, solidity, extent and sum of CCDCFD. In our study, Ranker (Hall *et al*., 2009) is used to rank features by their individual evaluations which helps to identify those extracted features that contribute positively in the classification process. Based on the scores obtained, all eleven features have exhibited positive contribution. Thus, all of them are adopted in our system.

Region area, border contact area and orientation are employed to differentiate the normal regions from the subdural and extradural regions. Region area is to differentiate high intensity noise which relatively small compared with the hemorrhagic regions. Border contact area is a measure of number of pixels contact with the skull. Border contact area is adopted based on the priori-knowledge that normal high intensity region such as falx, tentorium and noise having less contact with the skull. Orientation is used to measure the angle of the regions. The absolute value of orientation is considered only to differentiate the normal regions from subdural and extradural regions. Normally subdural and extradural possess higher degree of angle compared with the higher intensity normal brain tissue.

The subsequent eight features are primarily adopted to differentiate extradural from subdural. Extradural and subdural always appear to be bi-convex and elongated crescent in shape, respectively. Generally, extradural is more solid, extent, elliptic, circular and triangular as compared to subdural. However, subdural is more concave and linear than extradural. Based on these priori-facts, extent, solidity, ellipticity, circularity, triangularity, linearity, concavity and sum of CCDCFD are proposed to quantify the shape of extradural and subdural. Firstly, circularity (Zunic *et al*., 2010) is computed based on moments as given in Eq. 8:

$$\text{Circularity } \partial(\text{ROI}) = \frac{\left(u_{0,0}(\text{ROI})\right)}{2\pi\left(u_{2,0}(\text{ROI}) + u_{0,2}(\text{ROI})\right)} \quad (8)$$

where, the (i, j) is moment as defined in Eq. 9:

$$\mu_{i,j}(\text{ROI}) = \iint_{\text{ROI}} x^i y^j dxdy \quad (9)$$

For triangularity and ellipticity, the affine moment invariant used to characterise the triangle and ellipse is given in Eq. 10:

$$I = \frac{\mu_{2,0}(\text{ROI})\mu_{0,2}(\text{ROI}) - (\mu_{1,1}(\text{ROI}))^2}{(\mu_{0,0}(\text{ROI}))^4} \quad (10)$$

From the affine moment invariant, triangularity 12 and ellipticity 12 of a ROI are derived as shown in Eq. 11-12, respectively:

$$\text{Triangularity, } \angle(\text{ROI}) \begin{cases} 108I & \text{if } I \le \frac{1}{108} \\ \frac{1}{108I} & \text{otherwise} \end{cases} \quad (11)$$

$$\text{Ellipticity, } \ell(\text{ROI}) \begin{cases} 16\pi^2 I & \text{if } I \le \frac{1}{16\pi^2} \\ \frac{1}{16\pi^2 I} & \text{otherwise} \end{cases} \quad (12)$$

Linearity 13 that is used to represent the elongated shape of subdural is defined as in Eq. 13:

$$\text{Linearity, } L(\text{ROI}) = 1 - \frac{\text{minor axis}}{\text{major axis}} \quad (13)$$

where, the major and minor axes are the longest and shortest diameter of the ROI, respectively. Extent measures the ratio of the pixels within the region to the pixels in the bounding box. Solidity is used to measure proportion of the pixels in the convex hull that also in the region of interest. Besides we propose a new concavity measure to measure the degree of concaveness for subdural. This new concavity takes into consideration the contours and overlapping area in order to acquire the concave area. The derivation of the concavity is based on the following steps:

- Locate inner contour(without contact with skull) and outer contour(with contact with skull) as shown in Fig. 6b and c, respectively
- Locate the two endpoints of the inner contour and outer contour by using the 3×3 neighbourhood $(x_1^{outer}, y_1^{outer})$ $(x_2^{outer}, y_2^{outer})$, $(x_1^{inner}, y_1^{inner})$ $(x_2^{inner}, y_2^{inner})$
- Interpolate the linear line to connect the endpoints, $(x_1^{inner}, y_1^{inner})$ with $(x_2^{inner}, y_2^{inner})$ and $(x_1^{outer}, y_1^{outer})$ with $(x_2^{outer}, y_2^{outer})$ in order to generate the closed inner and outer contour based on Eq. 14 as shown in Fig. 6d and e:

$$y = y_1 + \frac{(x - x_1)(y_2 - y_1)}{(x_2 - x_1)} \quad (14)$$

Fill up the closed inner and outer contours by using morphological operation as shown in Fig. 6f and g. Acquire the concave area by overlapping the filled inner contour with filled outer contour as shown in Fig. 6h: Concave area = $A_{filled\_contour} \cap A_{filled\_inner}$. Divide the concave area by area of filled inner contour to normalize the concave area to the interval [0, 1]. With this, concavity of a ROI is defined as:

$$\text{Concavity, } \lambda(\text{ROI}) = \frac{A_{filled\_inner} \cap A_{filled\_outer}}{A_{filled\_inner}} \quad (15)$$

Last feature proposed to describe the extradural is the sum of CCDCFD. The sum of the CCDCFD specifies the symmetric property of the extradural. The more symmetrical the shape is the lower the sum of the CCDCFD will be.

In computing the sum of CCDCFD we only consider the first 32 Fourier coefficients from low frequency. This is because the information is concentrated at the low frequency. Besides, the remaining coefficients at high frequency are considered as a noise and are omitted in order to attain scale invariance, magnitudes of other coefficients are divided by magnitude of second Fourier coefficient. The scale invariant feature vector for the descriptor is given by Eq. 16. Besides, dividing by the magnitude of second Fourier coefficient will also normalize the range for sum of CCDCFD to [0, 1]. From the feature vector, the sum of CCDCFD is computed as in Eq. 17:

$$FV = \left\{ \left|\frac{ft(2)}{ft(1)}\right|, \left|\frac{ft(3)}{ft(1)}\right|, \ldots\ldots, \left|\frac{ft(N-2)}{ft(1)}\right|, \left|\frac{ft(N-1)}{ft(1)}\right| \right\} \quad (16)$$

$$\text{Sum of CCDCFD} = \sum_{k=2}^{N-1} \left|\frac{ft(k)}{ft(1)}\right| \quad (17)$$

where, Ft (k) is the function of the discrete Fourier transform (DFT)

RESULTS AND DISCUSSION

On overall, there are 519 CT brain images which consist of 156 normal slices, 217 intra-axial slices, 60 extradural slices and 86 subdural slices. This dataset is retrospectively extracted from over >70 patients from the CT archive of the two collaborating hospitals. On the average, around seven to eight slices have been utilized per patient. Basically this dataset is a mixture of normal slices and three kinds of different hemorrhage slices which are intra-axial, subdural and extradural hemorrhages.

Table 1: Recall and precision for non-intra-axial and intra-axial slices

Variables	Non-intra-axial slice	Intra-axial slice	Overall
Recall	0.954	0.793	0.886
Precision	0.865	0.925	0.890

Table 2: Recall and precision for subdural, extradural and normal regions

Variables	Normal region	Extradural region	Subdural region	Overall
Recall	0.925	0.850	0.892	0.906
Precision	0.922	0.927	0.858	0.907

For the classification, Support Vector Machine (SVM) with radial-basis function kernel is adopted as it yielded better results. During the classification, ten-fold cross validation method is performed on the 519 CT slices. The images are segregated into ten disjointed subsets randomly. Subsequently nine subsets are used for training and the remaining one subset is used for testing. Each disjointed subset plays the role as a new data set and is channeled into the SVM classifier during the classification. Finally, the results obtained from the ten fold validation are then combined to acquire the sole estimation.

For the classification of intra-axial slices, the 22 features which are extracted from the left and right hemispheres will be channeled into SVM classifier and results of the classification are depicted in Table 1. The classification for this stage is to distinguish the intra-axial hemorrhage slices from the other slices. As observed from Table 2, the adopted features generated acceptable results as the overall Correct Classification Rate (CCR) or recall is 0.886. As a matter of fact, recall rate is more useful to the medical doctors compared to the precision. This is because recall rate only indicates the correctly classified hemorrhage slices. In other words, recall rate never take the misclassified hemorrhage slices into consideration. However, precision is also needed here to reflect the false positive cases due to misclassification.

The CCR of intra-axial slice is approximately 0.8 which is relatively lower compared with CCR of non-intra-axial hemorrhage slices. This is due to the similarity of the features for some non-intra-axial and intra-axial slices which caused the misclassification. Some higher intensity normal regions presented in non-intra-axial slices caused some intra-axial slices to be grouped with them.

For the classification of subdural and extradural, the 11 features extracted from all the 417 boundary regions will be used to differentiate the normal, extradural and subdural regions. From Table 2, satisfactory results are obtained as on the overall CCR is over 0.9. The recall for normal regions is highest as it is easier to distinguish

normal regions as compared to extradural and subdural regions. Once a particular abnormal region is detected in a slice, the slice will be annotated accordingly. On overall, the CCR obtained for subdural and extradural slices is higher than intra-axial slices. This is due to the more specific local shape features adopted for subdural and extradural which results in better recognition. Global features are considered to annotate the intra-axial slices due to their arbitrary shapes.

CONCLUSION

In this study, we have presented an annotation system to classify the hemorrhage slices. Experimental evaluations have also been conducted over a dataset consisting of 519 CT slices to demonstrate the effectiveness and feasibility of our proposed system. The proposed method yields promising results where the correct classification rate for intra-axial, extradural and subdural is 0.793, 0.85 and 0.892, respectively.

REFERENCES

Chan, T., 2007. Computer aided detection of small acute intracranial hemorrhage on computer tomography of brain. Comput. Med. Imag. Graphics, 31: 285-298.

Chawla, M., S. Sharma, J. Sivaswamy and L.T. Kishore, 2009. A method for automatic detection and classification of stroke from brain CT images. Proceedings of the IEEE Annual International Conference on Engineering in Medicine and Biology Society (EMBC09), September 3-6, 2009, IEEE, Hyderabad, India, ISBN:978-1-4244-3296-7, pp: 3581-3584.

Gong, T., R. Liu, C.L. Tan, N. Farzad and C.K. Lee *et al*., 2007. Classification of CT brain images of head Trauma. Proceedings of the IAPR International Workshop on Pattern Recognition in Bioinformatics, October 1-2, 2007, Springer, Berlin, Germany, pp: 401-408.

Hall, M., E. Frank, G. Holmes, B. Pfahringer, P. Reutemann and I.H. Witten, 2009. The WEKA data mining software: An update. SIGKDD Explorat. Newslett, 11: 10-18.

Haralick, R.M., 1979. Statistical and structural approaches to texture. Proc. IEEE, 67: 786-804.

Liu, R., C.L. Tan, T.Y. Leong, C.K. Lee and B.C. Pang *et al*., 2008. Hemorrhage slices detection in brain CT images. Proceedings of the 19th International Conference on Pattern Recognition, December 8-11, 2008, Tampa, Florida, USA., pp: 1-4.

Liu, Y., N.A. Lazar, W.E. Rothfus, F. Dellaert and A. Moore *et al*., 2004. Semantic-Based Biomedical Image Indexing and Retrieval. In: Trends and Advances in Content-Based Image and Video Retrieval, Kriege, S. and Veltkamp (Eds.). Carnegie Mellon University, Pittsburgh, Pennsylvania, pp: 1-20.

Matesin, M., S. Loncaric and D. Petravic, 2001. A rule-based approach to stroke lesion analysis from CT brain images. Proceedings of the 2nd International Symposium on Image and Signal Processing and Analysis, June 19-21, 2001, Pula, Croatia, pp: 219-223.

Zunic, J., K. Hirota and P.L. Rosin, 2010. A Hu moment invariant as a shape circularity measure. Pattern Recognition, 43: 47-57.